Noise suppression of a dipole source by tensioned membrane with side-branch cavities

Y. Liu and Y. S. Choy[a)]
Department of Mechanical Engineering, The Hong Kong Polytechnic University, Hung Hom, Kowloon, Hong Kong SAR, China

L. Huang
Department of Mechanical Engineering, University of Hong Kong, Pokfulam Road, Hong Kong SAR, China

L. Cheng
Department of Mechanical Engineering, The Hong Kong Polytechnic University, Hung Hom, Kowloon, Hong Kong SAR, China

(Received 9 January 2012; revised 23 June 2012; accepted 26 June 2012)

Reducing the ducted-fan noise at the low frequency range remains a big technical challenge. This study presents a passive approach to directly suppress the dipole sound radiation from an axial-flow fan housed by a tensioned membrane with cavity backing. The method aims at achieving control of low frequency noise with an appreciable bandwidth. The use of the membrane not only eliminates the aerodynamic loss of flow, but also provides flexibility in controlling the range of the stopband with high insertion loss by varying its tension and mass. A three-dimensional model is presented which allows the performance of the proposed device to be explored analytically. With the proper design, this device can achieve a noise reduction of 5 dB higher than the empty expansion cavity recently proposed by Huang *et al*. [J. Acoust. Soc. Am. **128**, 152–163 (2010)]. Through the detailed modal analysis, even *in vacuo* modes of the membrane vibration are found to play an important role in the suppression of sound radiation from the dipole source. Experimental validation is conducted with a loudspeaker as the dipole source and good agreement between the predicted and measured insertion loss is achieved.
 [http://dx.doi.org/10.1121/1.4739448]

PACS number(s): 43.50.Gf, 43.55.Rg [NX] Pages: 1392–1402

I. INTRODUCTION

The ventilation and air-conditioning systems play an important role in providing comfortable environments, but there exist noise problems associated with the fan installations especially at low frequencies. The main mechanisms of the tonal fan noise are the interaction between the rotor and the stator and the interaction between the non-uniform inlet flow and the rotor blades, while broadband noise derives from the turbulence and/or separation flow condition of the rotor (Sharland, 1964). Trailing edge noise (Ffowcs Williams and Hall, 1970) and tip leakage flow (Dunne and Howe, 1997) also play an important role in both tonal and broadband radiation. At a low tip speed, a fan blade can be modeled as distributed dipole sources along its radial span. There are two components of the unsteady loading on the fan blades: thrust noise, which propagates along the duct, and drag noise in the circumferential direction. Installed inside an enclosure or a duct, only thrust noise with plane wave mode is radiated below the first cut-on frequency of the duct and with an anti-phase relation at the two sides of the dipole source.

The ducted fan noise can be controlled in the propagating path or directly on the noise source itself. In the first category, porous duct lining has been frequently utilized to absorb the noise, but there can be environmental problems when fibers are exposed to flow (Ackermann and Fuchs, 1989; Fuchs, 2001a, 2001b) and sound absorption for low frequency noise is ineffective. Expansion chambers or multiple chambers with perforated tubes are commonly employed for vehicles. Both sound reflection and absorption can be achieved but the device is normally bulky especially for the low frequencies (Selamet *et al*., 2005; Munjal, 1987). The concept of using an array of compact membrane absorbers and micro-perforated panel absorbers is also widely adopted in silencer's design at the downstream part of the source (Zha *et al*., 2002; Fuchs, 2001a, 2001b). In order to passively achieve broadband noise reduction without causing any extra noticeable pressure loss, Huang (2002) introduced the concept of drum silencer, which consists of an expansion chamber with two side-branch cavities covered by light membranes under high tension. The prototype device has been tested successfully without and with flow (Choy and Huang, 2002, 2005).

On the other hand, little attention has been devoted to the control of sound radiation by a dipole source, e.g., a fan. Although active control is a possible option (e.g., Wang *et al*., 2005; Wang and Huang, 2006), the need of the

a)Author to whom correspondence should be addressed. Electronic mail: mmyschoy@polyu.edu.hk

actuators and sensors leads to difficultly in implementation, and most importantly, its application is limited to the tonal noise. More relevant to the current study, Huang *et al.* (2010) recently proposed a passive method by creating a destructive acoustic interference between the sound fields at the two sides of the dipole source with anti-phase relationship. This can be achieved by housing the dipole source with the expansion chamber. Below the first cut-on frequency of the duct, there is significant acoustic interference between noise radiation from the dipole source and the reflections at the expanded duct junctions due to the change of the cross section area. In the real device tested, there was an acoustically transparent membrane covering the chamber so that the straight flow passage is preserved. The membrane has negligible tension and its mass is also very small. This configuration would work well only when the pressure rise across the fan is small, such as that produced by a small ventilation fan. For larger fans with substantial pressure rise, the membrane cannot sustain the pressure difference and it will either lead to a membrane breakdown or a large unwanted tension while diminishing the silencing performance. The motivation of this study is to investigate the performance of a new configuration in which a suitable membrane with a finite mass and pre-tension will produce good acoustic performance.

The new configuration is similar to the drum-like silencer but the physical mechanism behind is totally different. The present device aims at directly suppressing the sound radiation from dipole sources through its interaction with the membrane vibration, while a drum-silencer, which is installed downstream, relies on reflecting sound back to the source along the propagating path. This study focuses on developing a theoretical model which allows a thorough analysis on sound cancellation mechanism and prediction of its performance. The proposed theoretical model has the following distinct features. (a) It is different from traditional monopole incident sound wave assumption (Lawrie and Guled, 2006; Selamet *et al.*, 2005), a dipole source is considered, which is a better representation of the fan blade source. (b) In order to simulate a realistic ducted fan with short duct length, multiple reflections due to two openings are considered. This is drastically different from traditional theoretical model dealing with silencers of infinite length. The response of the membrane is fully coupled with the acoustic waves in the duct and cavity. The aim of this device is to achieve desirable noise reduction over a wide frequency range covering the blade passing frequencies (BPF) under different rotational speeds.

In what follows, Sec. II proposes a three-dimensional (3D) analytical model in detail. In Sec. III, experimental study is conducted to validate the theoretical model by using a loudspeaker as the dipole source.

In this section, the optimization procedure is also applied and the noise reduction mechanism is discussed. In Sec. IV, the main conclusions are summarized.

II. THEORY

This section outlines the theoretical formulation used to predict the insertion loss of the proposed device. It begins with the description of a general theoretical model for the coupled dynamics of two-dimensional membranes in a 3D duct and cavity. It is presented following standard Galerkin procedure. The resulting set of linear equations is solved by general matrix inversion techniques.

A. The 3D model

The configuration under investigation is shown in Fig. 1. It has a 3D rectangular duct of height h^* and width w^* installed with two rigid cavities of length L_c^* and depth h_c^* on two opposite sides. The cavities are covered with two membranes of length L^* and width w^* which form part of the otherwise rigid duct. A dipole source which is used to simulate fan noise is located at the mid-point of the membranes; $x^* = 0.5\,L^*$, $y^* = 0.5\,w^*$, and $z^* = 0.5\,h^*$. The upstream and downstream duct connecting to the leading edge and trailing edge of the membrane has the length of L_u^* and $L_d^* - L_c^*$, respectively. The membranes are fixed at the leading and trailing edges at $x^* = 0, L^*$, as well as at the other two edges

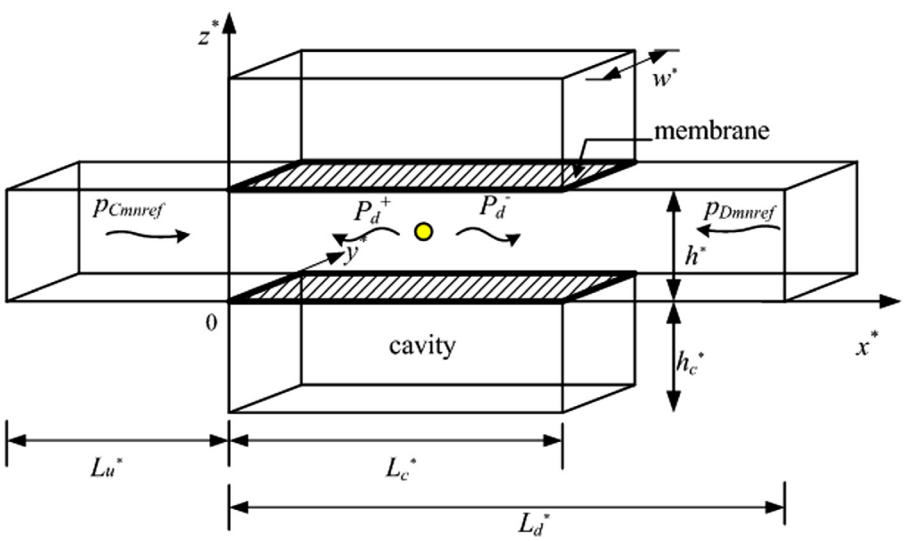

FIG. 1. (Color online) 3D theoretical model of the dipole noise control by tensioned membrane backed with cavity.

at $y^* = 0$, w^*. For convenience, all variables are nondimensionalized as follows by three basic quantities, air density ρ_0^*, duct height h^*, and speed of sound in free space c_0^*:

$$x = \frac{x^*}{h^*}, \quad y = \frac{y^*}{h^*}, \quad z = \frac{z^*}{h^*}, \quad t = \frac{c_0^* t^*}{h^*}, \quad h_c = \frac{h_c^*}{h^*},$$
$$L = \frac{L^*}{h^*}, \quad L_c = \frac{L_c^*}{h^*}, \quad f = \frac{f^* h^*}{c_0^*}, \quad \omega = \frac{\omega^* h^*}{c_0^*},$$
$$k_0 = 2\pi f, \quad m = \frac{m^*}{\rho_0^* h^*}, \quad T = \frac{T^*}{h^* w^* \rho_0^* (c_0^*)^2},$$
$$F = \frac{F^*}{h^* w^* \rho_0^* (c_0^*)^2}, \quad p = \frac{p^*}{\rho_0^* (c_0^*)^2}.$$

Here, m is the membrane-to-air mass ratio, T is the tension of the membrane, F is the concentrated force exerted on the fluid by the dipole source, p is the sound pressure. Assuming that $h = w$, based on such a normalization scheme, the first cut-on frequency of the rigid-walled duct is $f = 0$.

In Fig. 1, dipole sound waves p_d are radiated from the source to the upstream and downstream sides which are denoted by p_d^- for $x < 0.5L$ and p_d^+ for $x > 0.5L$, respectively (Rodarte and Miller, 2001).

$$p_d^{\pm} = \sum_{n=0}^{\infty}\sum_{m=0}^{\infty} \frac{\pm F}{(2A_{ym}A_{zn})} \cos\left(\frac{m\pi}{2}\right)\cos\left(\frac{n\pi}{2}\right) \times \cos(m\pi y)\cos(n\pi z) e^{\mp i k_{mn}(x-0.5L)},$$
$$c_{mn} = \frac{i}{\sqrt{(m\pi/\omega)^2 + (n\pi/\omega)^2 - 1}}, \quad k_{mn} = \frac{\omega}{c_{mn}},$$
$$A_{ym} = \begin{cases} 1, & m = 0 \\ 1/2, & m > 0 \end{cases}, \quad A_{zn} = \begin{cases} 1, & n = 0 \\ 1/2, & n > 0 \end{cases}, \tag{1}$$

where ω is the angular frequency, c_0 is the speed of sound, and m, n are integers. Note that p_d^+, p_d^- are for radiations in rigid-wall duct, which are superimposed by membrane responses described below.

These waves excite the membrane into vibration with a transverse displacement $\eta(x, y)$ in the z direction with velocity $V = i\omega\eta$. The vibrating membrane will radiate sound waves which impose a radiation pressure on the membrane surface. There is high coupling between the acoustic waves and membrane vibration.

The vibration of the lower membrane with its nominal position at $z = 0$ is governed by

$$m\frac{\partial^2 \eta}{\partial t^2} - T_x \frac{\partial^2 \eta}{\partial x^2} - T_y \frac{\partial^2 \eta}{\partial y^2} + (p_d^+ + p_d^- + \Delta p) = 0, \tag{2}$$

where T_x, T_y are the tensile forces applied in the axial and lateral directions, respectively, Δp is the fluid loading on the upper and lower sides of the membrane induced by the membrane vibration itself. Structural damping in such a thin membrane is normally very small and is ignored. The solution for the problem with two identical membranes is simplified to a problem in which one membrane is installed in a duct of height $h/2$ and the symmetric plane of $z = h/2$ is replaced by a solid wall.

B. Modal dynamics of the sound-membrane interaction

The standard Galerkin procedure is utilized to solve the coupled problem between the sound membrane interactions. For membranes fixed on all four edges with harmonic vibration, the membrane vibration velocity V is expressed as a combination of *in vacuo* vibration modes such that

$$V(x,y) = \frac{\partial \eta(x,y)}{\partial t} = e^{i\omega t}\sum_{j=1}^{\infty}\sum_{l=1}^{\infty} V_{jl}\sin(j\pi\xi)\sin(l\pi\varsigma),$$
$$V_{jl} = 4\int_0^1\left[\int_0^1 V\sin(j\pi\xi)\sin(l\pi\varsigma)d\xi\right]d\varsigma, \tag{3}$$

where j, l are modal index in the x and y direction, respectively, and $\xi = x/L$ and $\varsigma = y/w$ are the local axial coordinates. Then Eq. (2) becomes

$$\mathcal{L}_{jl}V_{jl} + 4\int_0^1\int_0^1 (p_d^+ + p_d^- + \Delta p)\sin(j\pi\xi)\sin(l\pi\varsigma)\,d\xi\,d\varsigma = 0, \tag{4}$$

where $\mathcal{L}_{jl} = mi\omega + (T_x/i\omega)(j\pi/L)^2 + (T_y/i\omega)(l\pi/w)^2$ is the structural property of the membrane. The fluid loading Δp is found by decomposing the membrane vibration into various *in vacuo* modes with modal vibration velocity amplitude V_{jl}

$$\Delta p = \sum_{j=1}^{\infty}\sum_{l=1}^{\infty} V_{jl}\,p_{jl}^{(1)}, \tag{5}$$

where $p_{jl}^{(1)}$ is the fluid loading caused by the modal vibration of unit amplitude of $V = \sin(j\pi\xi)\sin(l\pi\varsigma)$. The vibration of mode jl causes loading on all other *in vacuo* modes, say $j'l'$, and the modal impedance is defined and calculated as

$$Z_{jlj'l'} = 4\int_0^1\int_0^1 p_{jl}^1\sin(j'\pi\xi)\sin(l'\pi\varsigma)\,d\xi\,d\varsigma, \tag{6}$$

where j and l denote the source vibration mode, while j' and l' denote the resulting mode indices. A detailed method of solution to determine the modal impedance was given in Huang (2005).

The fluid loading Δp is divided into three parts

$$\Delta p = p_{\text{rad}} + p_{\text{ref}} - p_{\text{cav}}, \tag{7}$$

where p_{rad} is the radiation sound pressure in the main duct on the upper surface of the membrane at $z = 0+$ excluding sound reflections by the two outlets, p_{ref} is the sound reflected by the open ends of the main duct, and p_{cav} is the pressure inside the cavity acting on the lower surface of the membrane at $z = 0$-. The formulation for p_{rad} is well-known (Doak, 1973), and is rewritten in dimensionless form

$$p_{\text{rad}}(x,y,z) = \frac{L}{2}\sum_{m=0}^{\infty}\sum_{n=0}^{\infty} c_{mn}\psi_{mn}(y,z)\int_0^1\int_0^1 \psi_{mn}(y',z') \times V(x',y')\times[H(x-x')e^{-ik_{mn}(x-x')} + H(x'-x)e^{+ik_{mn}(x-x')}]\,d\xi'\,d\varsigma', \tag{8}$$

where H is the Heaviside function, c_{mn}, k_{mn}, and ψ_{mn} are, respectively, the modal phase speed, the modal wave number, and the modal velocity potential

$$\psi_{mn} = \sqrt{2-\delta_{0m}}\sqrt{2-\delta_{0n}}\cos(m\pi y)\cos(n\pi z),$$

and δ_{0n} is the Kronecker delta. For a prescribed modal vibration of a unit amplitude, the corresponding impedance of the radiation from the membrane $z=0+$ is given as

$$\begin{aligned} Z_{\mathrm{rad},jlj'l'} &= 4\int_0^1\int_0^1 p_{\mathrm{rad}}\sin(j'\pi\xi)\sin(l'\pi\varsigma)d\xi d\varsigma \\ &= 2L\sum_{m=0}^{\infty}\sum_{n=0}^{\infty} c_{mn}(2-\delta_{0m})(2-\delta_{0n}) \\ &\quad\times\left(\frac{l\pi(1-\cos(l\pi)\cos(m\pi))}{(l\pi)^2-(m\pi)^2}\right) \\ &\quad\times\left(\frac{l'\pi(1-\cos(l'\pi)\cos(m\pi))}{(l'\pi)^2-(m\pi)^2}\right)I_{j,j'}, \end{aligned} \tag{9}$$

where

$$\begin{aligned} I_{j,j'} &= \frac{j\pi j'\pi[(\cos(j\pi)+\cos(j'\pi))(\cos(j\pi)-e^{-ik_{mn}L})]}{[(k_{mn}L)^2-(j\pi)^2][(k_{mn}L)^2-(j'\pi)^2]} \\ &\quad-\frac{ik_{nm}L\delta_{jj}}{(k_{mn}L)^2-(j\pi)^2}. \end{aligned} \tag{10}$$

Similarly, the acoustic pressure in 3D configuration inside a lightly damped cavity with length L_c, height h_c, and width w (here $L_c=L$) can be obtained through the cavity mode decomposition (Kuttruff, 2000)

$$\begin{aligned} p_{\mathrm{cav}}(x,y,z) &= \sum_{r,s,t}^{\infty}\frac{-i\omega\phi_{rst}(x,y,z)}{L_c h_c w(\kappa_{r,s,t}^2-k_0^2+2i\zeta_{r,s,t}\kappa_{r,s,t}k_0)} \\ &\quad\times\int_0^{L_c}\int_0^{w} V(x',y',z')\phi_{rst}(x',y',z')\,dx'\,dy', \end{aligned} \tag{11}$$

where $\zeta_{r,s,t}$ is the damping ratio of the (r,s,t)th acoustic mode $\phi_{rst}(x,y,z)$, $\kappa_{r,s,t}$ is the corresponding acoustic wave number, given as

$$\begin{aligned} \phi_{rst}(x,y,z) &= \sqrt{(2-\delta_{0r})(2-\delta_{0s})(2-\delta_{0t})} \\ &\quad\times\cos\left(\frac{r\pi x}{L_c}\right)\cos\left(\frac{s\pi y}{w}\right)\cos\left(\frac{t\pi z}{h_c}\right), \\ \kappa_{rst} &= \sqrt{\left(\frac{r\pi}{L_c}\right)^2+\left(\frac{s\pi}{w}\right)^2+\left(\frac{t\pi}{h_c}\right)^2}. \end{aligned}$$

Therefore, the cavity pressure induced by the jth and lth modal vibration of unit amplitude can be obtained, hence the corresponding modal impedance becomes

$$\begin{aligned} Z_{\mathrm{cav},jlj'l'} &= 4\int_0^1\int_0^1 p_{\mathrm{cav}}(x,y)\sin(j'\pi\xi)\sin(l'\pi\varsigma)\,d\xi\,d\varsigma \\ &= 4\sum_{r=0}^{\infty}\sum_{s=0}^{\infty}\sum_{t=0}^{\infty}\frac{-i\omega(2-\delta_{0r})(2-\delta_{0s})(2-\delta_{0t})}{L_c h_c w(\kappa_{r,s,t}^2-k^2+2i\zeta_{r,s,t}\kappa_{r,s,t}k)} \\ &\quad\times\frac{j\pi(1-\cos(j\pi)\cos(r\pi))}{(j\pi)^2-(r\pi)^2} \\ &\quad\times\frac{l\pi(1-\cos(l\pi)\cos(s\pi))}{(l\pi)^2-(s\pi)^2} \\ &\quad\times\frac{j'\pi(1-\cos(j'\pi)\cos(r\pi))}{(j'\pi)^2-(r\pi)^2} \\ &\quad\times\frac{l'\pi(1-\cos(l'\pi)\cos(s\pi))}{(l'\pi)^2-(s\pi)^2}. \end{aligned} \tag{12}$$

The reflections p_{ref} in the relatively short duct are formed from two sound wave reflection with modal function due to open end condition at the outlets. The waves reflected from upstream and downstream are denoted as R_{mn}^u and R_{mn}^d, respectively.

$$p_{\mathrm{ref}} = R_{mn}^u e^{-ik_{mn}x} + R_{mn}^d e^{+ik_{mn}x}.$$

By considering exit boundary at the downstream duct with a distance L_d from the origin and that at the upstream duct with a distance L_u, the relationship between the waves can be expressed in term of reflection coefficient β,

$$\frac{R_{mn}^d e^{ik_{mn}L_d}}{p_d^+|_{x=L_d}+p_{\mathrm{rad}}|_{x=L_d}+R_{mn}^u e^{-ik_{mn}L_d}} = \beta \text{ and}$$

$$\frac{R_{mn}^u e^{ik_{mn}L_u}}{p_d^-|_{x=L_u}+p_{\mathrm{rad}}|_{x=-L_u}+R_{mn}^d e^{-ik_{mn}L_u}} = \beta,$$

where $\beta=(Z-1)/(Z+1)$ and $Z=(ka)^2/2+ika(8/3\pi)$ for open end with unflange condition (Levine and Schwinger, 1948).

Hence,

$$R_{mn}^u = \frac{\beta^2 e^{-ik_{mn}L_u}(p_d^+|_{x=L_d})+\beta e^{ik_{mn}L_d}(p_d^-|_{x=-L_u})+\beta^2 e^{-ik_{mn}L_u}p_{\mathrm{rad}}|_{x=L_d}+\beta e^{ik_{mn}L_d}p_{\mathrm{rad}}|_{x=-L_u}}{(e^{ik_{mn}(L_u+L_d)}-\beta^2 e^{-ik_{mn}(L_d+L_u)})}, \tag{13}$$

$$R_{mn}^d = \frac{\beta e^{ik_{mn}L_u}(p_d^+|_{x=L_d})+\beta^2 e^{-ik_{mn}L_d}(p_d^-|_{x=-L_u})+\beta e^{ik_{mn}L_u}(p_{\mathrm{rad}}|_{x=L_d})+\beta^2 e^{-ik_{mn}L_d}(p_{\mathrm{rad}}|_{x=-L_u})}{(e^{ik_{mn}(L_d+L_u)}-\beta^2 e^{-ik_{mn}(L_u+L_d)})}. \tag{14}$$

The formation of the reflection sounds comes from the direct radiation from the dipole source and radiation sound from the membrane. Therefore the modal impedance of the reflection sound waves p_{ref} becomes

$$
\begin{aligned}
Z_{\text{ref},jlj'l'(\text{total})} &= 4\int_0^1\int_0^1 [R^u_{mn}(x,y)+R^d_{mn}(x,y)]\sin(j'\pi\xi)\sin(l'\pi\varsigma)\,d\xi\,d\varsigma \\
&= \left.\begin{aligned}
&\frac{\beta}{\left(e^{ik_{mn}(L_d+L_u)}-\beta^2 e^{-ik_{mn}(L_d+L_u)}\right)}\sum_{m=0}^{\infty}\sum_{n=0}^{\infty}\frac{C_{mp}F\cos\left(\frac{m\pi}{2}\right)\cos\left(\frac{n\pi}{2}\right)}{2A_{ym}A_{zn}} \\
&\times[(-\beta e^{-ik_{mn}(L_u+L_d)}+e^{ik_{mn}(L_d-L_u)})R_{rad,j}+(e^{-ik_{mn}(L_d+L_u)}-\beta e^{-ik_{mn}(L_u+L_d)})R_{\text{ref},j}]
\end{aligned}\right\} I_{d,\text{ref}} \\
&\quad \left.\begin{aligned}
&+\frac{2L_c\beta}{\left(e^{ik_{mn}(L_d+L_u)}-\beta^2 e^{-ik_{mn}(L_d+L_u)}\right)}\sum_{m=0}^{\infty}\sum_{n=0}^{\infty}c_{mn}(2-\delta_{0m})(2-\delta_{0n})C_{mp}C_{mp'} \\
&\times[(e^{-ik_{mn}(L_d+L_u)}\beta R_{\text{ref},j}+(e^{ik_{mn}(L_d-L_u)})R_{\text{rad},j})R_{\text{rad},j'} \\
&+((e^{-ik_{mn}(L_d-L_u)})R_{\text{ref},j}+e^{-ik_{mn}(L_d+L_u)}\beta R_{\text{rad},j})R_{\text{ref},j}]
\end{aligned}\right\} Z_{\text{ref},jl,j'l'},
\end{aligned}
\tag{15}
$$

where

$$
\begin{aligned}
R_{\text{rad},j} &= \frac{j\pi(1-e^{-ik_{mn}L}\cos(j\pi))}{(j\pi)^2-(k_{mn}L)^2}, \\
R_{\text{ref},j} &= \frac{j\pi(1-e^{ik_{mn}L}\cos(j\pi))}{(j\pi)^2-(k_{mn}L)^2},
\end{aligned}
\tag{16}
$$

$$
\begin{aligned}
C_{ml} &= \frac{l(1-\cos(l\pi)\cos(m\pi))}{\pi(l^2-m^2)}, \\
C_{ml'} &= \frac{l'(1-\cos(l'\pi)\cos(m\pi))}{\pi(l'^2-m^2)}.
\end{aligned}
\tag{17}
$$

The first term of Eq. (15) stands for the modal impedance of the reflection waves of the direct radiation from the dipole source $I_{d,\text{ref}}$, while the latter term stands for that of the radiation from the panel $Z_{\text{ref},jl,jl'}$.

C. Panel response and insertion loss

Having found the modal radiation, cavity reflection, and duct reflection due to open end conditions, the dynamics equation (4) can be cast as a truncated set of linear equations for modal vibration amplitudes, V_{jl},

$$
\begin{aligned}
&\mathcal{L}_{jl}V_{jl}+\sum\sum_{j,l,j',l'}[Z_{\text{rad}\,jlj'l'}+Z_{\text{cav}\,jlj'l'}+Z_{\text{ref}\,jlj'l'}]V_{jl} \\
&\quad = -(I_d+I_{d,\text{ref}})_{jl},
\end{aligned}
\tag{18}
$$

where

$$
I_d = 4\int_0^1\int_0^1 (p_d^- + p_d^+)\sin(j'\pi\xi)\sin(l'\pi\varsigma)\,d\xi\,d\varsigma. \tag{19}
$$

Hence,

$$
\begin{aligned}
I_d &= \frac{4p(1-\cos(p\pi)\cos(m\pi)}{\pi(p^2-m^2)} \\
&\quad\times\sum_{m=0}^{\infty}\sum_{n=0}^{\infty}\frac{F_x\cos\left(\frac{m\pi}{2}\right)\cos\left(\frac{n\pi}{2}\right)}{2A_{ym}A_{zn}} \\
&\quad\times\frac{2\pi j\cos\left(\frac{j\pi}{2}\right)-e^{\frac{-ik_{mn}L}{2}}\pi j(1+\cos(j\pi))}{(j\pi)^2-(k_{mn}L)^2}.
\end{aligned}
\tag{20}
$$

For the above calculation, the number of mode of the impedance matrix has to be truncated and the solution should be scrutinized in order to ensure the convergence of the solution. Denoting the axial number and lateral number of modes required by N_j and N_l, respectively, it is found that more transverse modes are needed when T_y is very low. $N_j = 20$ and $N_l = 40$ are normally enough as further increase in N does not make any noticeable difference. Having obtained the modal response of the membrane, the total sound pressure at the boundaries of the two exits $x = -L_u$ and $x = L_d$ of the duct can be found as follows:

$$
p_t|_{x=-L_u} = R^u_{mn}(1+\beta^{-1}) \text{ and } p_t|_{x=L_d} = R^d_{mn}(1+\beta^{-1}), \tag{21}
$$

respectively. For the special case with two anechoic terminations, the final sound pressure at the exit is found by simply adding the directly radiated waves from the dipole p_d to the far-field radiation waves p_{rad} which can be found from Eq. (8) taking only the plane wave mode $m = 0$ and $n = 0$. At the two ends, in the current study, an insertion loss (IL) is defined as the level difference of the acoustical power radiated from the unsilenced and silenced system. The unsilenced system is a straight duct with the same uniform cross section area s and total length. The dipole source is kept at the same position that is located in the center of the duct. Thus, the IL at $x = -L_u$ and $x = L_d$ is found as

$$
\text{IL} = 10\log_{10}\frac{\int|p_t|^2 ds|_{\text{original}}}{\int|p_t|^2 ds|_{\text{silenced}}}, \tag{22}
$$

where s is the cross section area.

III. RESULTS AND DISCUSSION

A. Experimental validation

Experiment is conducted to validate the proposed 3D theoretical model. The experimental setup is illustrated in Fig. 2. The duct used had a dimension of $h^* = 10$ cm by $w^* = 10$ cm cross section, the membrane had a length of $L^* = 3h^* = 0.3$ m, and the cavity depth of $h_c^* = 2h^* = 20$ cm. The first cut-on frequency in the duct is about 1700 Hz. The membrane was made of stainless steel, and the ratio of membrane to air mass calculated by $(m^*/\rho_0^* h^*)$ was 1.4. An optimal design will be performed in Sec. III B. The membranes were clamped and stretched by a specially designed tensile machine. One end of the membrane was fixed by two metal plates and the other end was stretched and ran through a very small slit, to be fixed by another two plates outside the duct and attached to a moveable tensile machine, for which the design details were given in Choy and Huang (2002, 2005). The width of the membrane was slightly wider than that of the duct, and the lateral edges of each membrane were inserted into a very thin gap between the two constituent plates of the cavity walls. The gap was less than 0.5 mm and had a depth of around 2 mm. The lateral edges were then glued and fixed by a very thin tape along the axial direction to minimize the acoustical leakage. The tensile force T_x was applied only in the axial direction and was measured by a strain gauge glued to the surface of the membrane. The strain gauge sensor (FLA-3-11-1Lt, Tokyo Sokki Kenkyujo Co., Ltd, Japan) had a dimension of 6 mm × 3 mm and its attachment could not cause noticeable influence on the dynamics of the stretched membrane. No tension was applied on the membrane in the lateral direction.

As shown in Fig. 2, a small loudspeaker of 75 mm in diameter was utilized to simulate the dipole sound source. The loudspeaker was held as a cantilever by a very rigid rod and located at the center of the duct. The radiated noise was measured at 20 cm from the outlet of the duct with an angle of $\theta = 30°$ from center line. One pair of 1/2-in. microphones [B&K type 4189 (Brüel & Kjaer), Denmark] were used and supported by Nexus Conditioning Amplifier type 2693, (Brüel & Kjaer), Denmark. The loudspeaker was driven by a function generator (Hioki 7075, Hioki E. E. Corporation, India) via a power amplifier [B&K Type 2716 C (Brüel & Kjaer), Denmark] at discrete frequencies from 120 Hz up to 1500 Hz with an interval of 10 Hz. The signals from the microphones were acquired through analog-to-digital converter (NI DAQ Card 6062 E, National Instrument Corporation, Austin) with MATLAB program. Finally, the sound pressures were directly measured at the exits at the upstream and downstream duct, denoted by p_{up} and p_{dn}, respectively.

In reality, the sound radiation from the loudspeaker is not an ideal dipole. Reflected sound is also scattered by the loudspeaker surface and the junctions between the interface at the rigid wall and flexible membrane. The sound radiation of the noise source is considered to consist of two components: one dipole with anti-phase relation and another monopole with in-phase relation. Apart from this, the measurement at one point at the upstream outlet will be contaminated by the sound pressure at the downstream outlet. Therefore, there was a need to extract the dipole component from the real noise source during the signal processing. We follow the sound wave decomposition procedure developed by Huang *et al.* (2010).

The membrane was applied with the dimensionless tension of 0.16 (the dimensional tensile force: 240 N). Focusing on the experimental data for the loudspeaker test, the spectrum of the extracted dipole radiation p_{upd} at the upstream for the straight duct without silencing treatment is shown in Fig. 3(a) as the dashed line, and that for the tensioned membrane housing as solid line, with arbitrary reference value for 0 dB. The lower frequency limit is restricted to the deficiency of small loudspeaker performance, while the upper limit of the frequency shown is 1000 Hz which is lower than the first cut-on frequency. The sound pressure level radiated from the straight duct is generally higher than that from the tensioned membrane housing, especially within the frequency range of 280 Hz to 800 Hz. The insertion loss under the extraction scheme measured at upstream IL_{upd} is shown in Fig. 3(b) as the open circle, while the prediction IL in Eq. (22) for the pure dipole source is depicted as dashed line

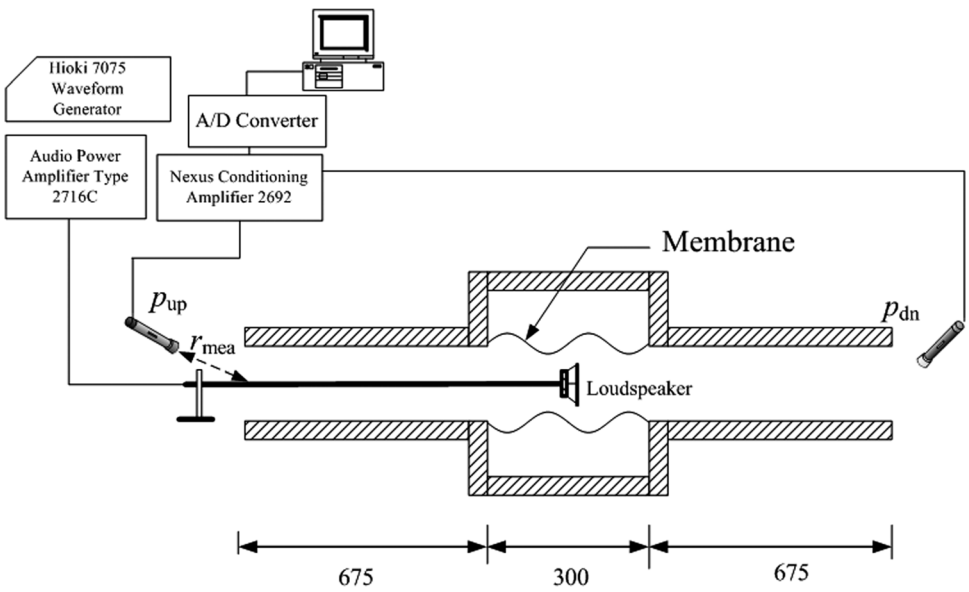

FIG. 2. Experimental setup for measuring the actual sound pressure radiated at the outlet by using two microphones at two exits of the duct.

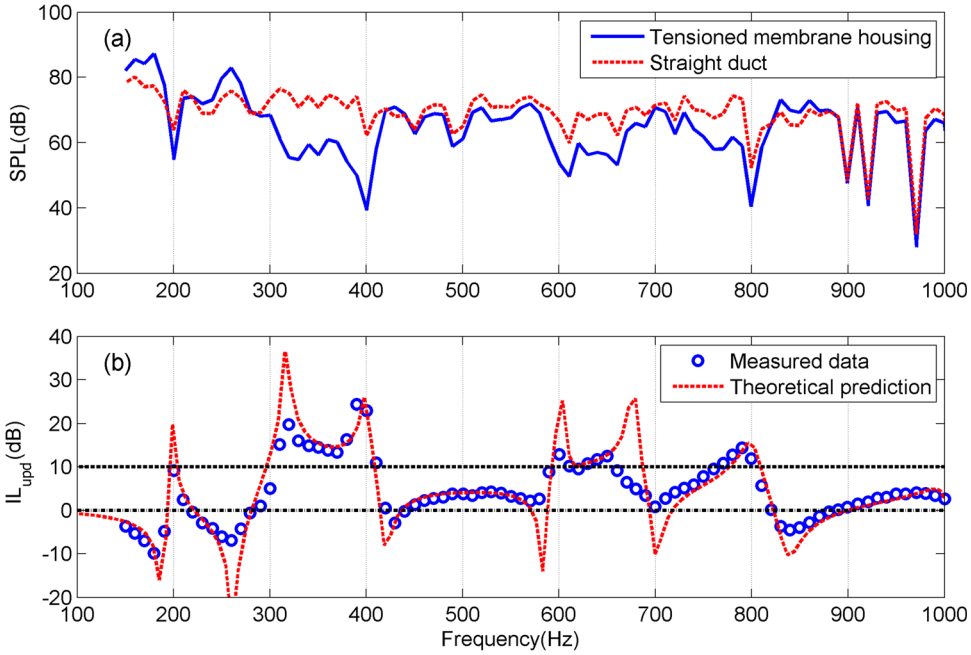

FIG. 3. (Color online) Comparison between the theoretical prediction and the experiment using a dipole source. (a) Spectra of the dipole sound radiation. (b) Comparison of the measured insertion loss (IL_{upd}) with dipole extraction (open circles) and analytical prediction (dashed line) for the finite rig with sound reflection at the open end.

for comparison. The agreement between them is generally satisfactory in terms of the overall IL level and the spectral pattern, although the experimental result is smooth at the peak and trough points. This leads to some deviations near the peak frequencies ($f = 300$ Hz and 660 Hz) and the trough frequencies ($f = 185$ Hz, 260 Hz, 418 Hz, 538 Hz, and 693 Hz). The main reason possibly comes from the energy dissipation of the lateral edge treatment, which was excluded in the calculation. On average, the IL is about 15 dB and 8 dB in the frequency range of 300 Hz to 400 Hz and 590 Hz to 800 Hz, respectively. These two frequency ranges are expected to cover the first two BPFs of an axial flow fan noise.

B. Parametric investigation for the structural property of the membrane

Having conducted the validation of the theory by experiment, the theoretical modeling is used to perform further analysis. It is anticipated that after using the tensioned membrane housing, the sound radiation from the dipole sound source can be well reduced in a desirable frequency range. To do this, the optimal performance of the device will be evaluated by finding the maximum logarithmic width of its stopband, which is defined as the frequency range in which the IL is everywhere equal to or greater than a pre-set criterion level (IL_{cr}). Thus, the optimization criterion can be expressed symbolically by $IL \geq IL_{cr}$, $f \in [f_1, f_2]$, $f_b = f_2/f_1$, the ratio of the frequency, defines the stopband. And the criterion level IL_{cr} is defined as the maximum IL, which is obtained from an empty expansion chamber with the same cross section area of the proposed device. The design of such a device involves many variables, for which a parametric study has to begin with fixing most variables. The cavity geometry is first assumed to be $h_c = 2$ and $L_c = 3$ for which IL_{cr} is 9.6 dB. The value of 9.6 dB is about the maximum IL of expansion chamber with expansion ratio of 5 in the numerical simulation. For a given mass ratio of the membrane, the maximum f_b is to be achieved by searching for the optimal tension T_{opt}. The target stopband should cover the first BPF of the low speed axial flow fan which is normally below $f = 0.15$ (dimensional: 515 Hz) and carries most energy. The tensile force in transverse direction is assumed to be zero during the parametric investigation.

Results of the performance optimization are shown in Fig. 4, in terms of the optimal axial tension T_{opt} as a function of m. Roughly speaking, T_{opt} keeps more or less constant when $m \leq 0.6$ and then decreases sharply to a very low value when $m = 0.65$. Figures 4(b) and 4(c) show the corresponding maximum bandwidth and the lower band limit as a function of m at the optimal tensions. As displayed in Fig. 4(b),

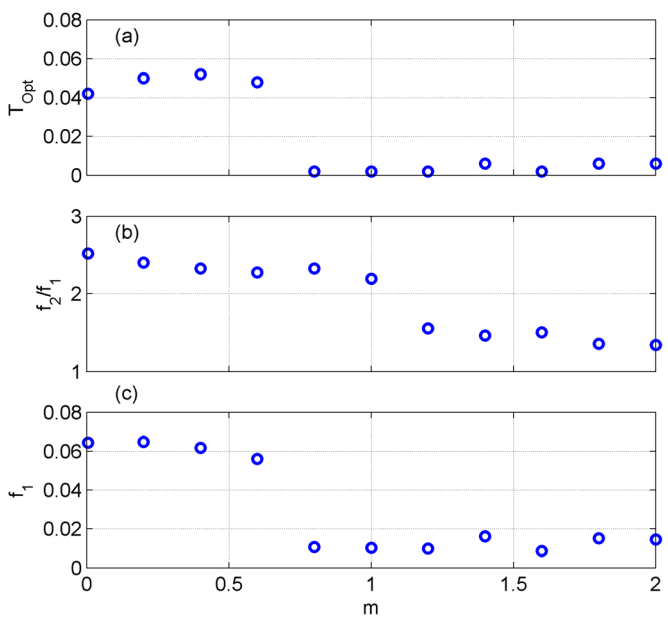

FIG. 4. (Color online) Performance optimization of the proposed device for the logarithmic bandwidth (a) the variation of the optimal tension T_{opt}, (b) ratio of frequency limits $f_b = (f_2/f_1)$, and (c) dimensionless lower band limit f_1 with the mass ratio (m).

the maximum achievable bandwidth f_b decreases gradually when the membrane mass increases. When the mass ratio m is less than unity, the bandwidth f_b can be kept at least 2.15, which is still larger than one octave band. It can be seen from Fig. 4(c) that f_1 decreases with m. This contrasts with the increment of f_1 for the performance of plate silencer with monopole source at the upstream (Wang *et al.*, 2007). Besides, f_1 falls strikingly from 0.06 to a very low level of 0.01 as m reaches 0.8. Therefore, the result of the drop of f_1 corresponds with the decrease of T_{opt}. The present device with $L_c = 3$ is effective to control the first BPF of axial-flow fan below $f = 0.14$ when the mass ratio is low enough to support $f_2/f_1 > 2$. Both f_b and f_1 remain almost constant when $0 \le \text{m} \le 0.6$. When the mass is too heavy, the membrane tends to be a part of rigid duct and prohibits the sound penetration into the cavity, thus sound radiation will propagate toward the duct exits directly. The optimal mass range of the membrane is finally found to be $0.2 \le \text{m} \le 0.6$.

C. Optimal results

Figure 5 shows the result for the default configuration with optimal structural parameter ($m = 0.4$ and $T_{\text{opt}} = 0.05$). Figure 5(a) shows the comparison of the theoretical IL_∞ spectra of the current device (solid line) with tensioned membrane with optimal performance and that of the empty expansion chamber without membrane (dashed dotted line) when the main duct has infinite length. The subscript with the symbol ∞ means the outlets of the duct are anechoic terminations. The horizontal dashed line is the reference level 9.6 dB, which is also the maximum IL_∞ for the expansion chamber with the same size. Notice that there is a sharp peak

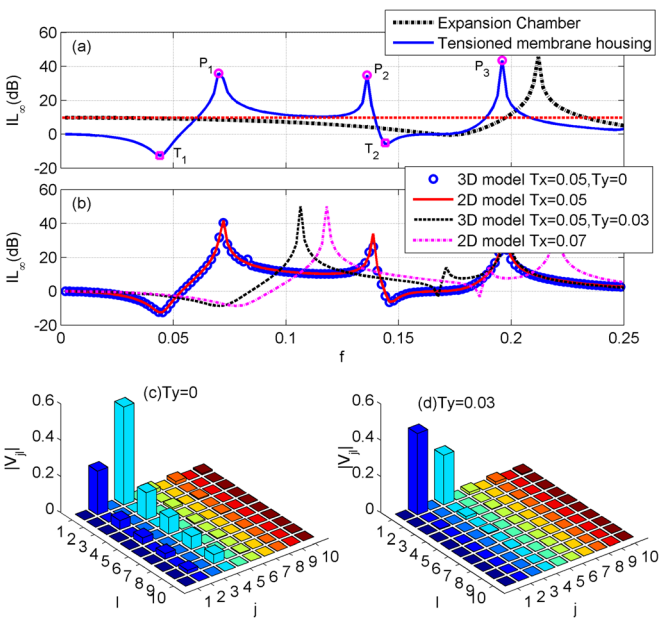

FIG. 5. (Color online) Performance of tensioned membrane housing at optimal axial tension. (a) Comparison of the IL spectra between the tensioned membrane housing with the optimal tension and the expansion chamber. (b) Comparison of the optimal IL spectrum for the 2D configuration with the 3D configuration. (c) The distribution of *in vacuo* modal vibration amplitude in 3D model with zero lateral tension on the membrane ($T_y = 0$). (d) The distribution of *in vacuo* modal vibration amplitude in 3D model with lateral tension ($T_y = 0.03$).

at $f = 0.21$ due to the high order modes in the expansion chamber. Concerning the performance of the present device with optimal tension, the lower and upper band limits are found to be $f_1 = 0.062$ and $f_2 = 0.145$, respectively, and this gives a width of $f_b = 2.35$ that is still attractive. Roughly speaking, the present device outperforms that of the empty expansion chamber by at least about 5 dB in this frequency range. In addition, three peaks at $f = 0.07$(P1), 0.136(P2), 0.196(P3) and two troughs at $f = 0.044$(T1), 0.146(T2) are observed and these can be explained by modal analysis and structural impedance in Secs III E.

D. The effect of lateral tension

When a low transverse tension T_y is present, the system becomes truly 3D. Figure 5(b) shows the comparison of IL_∞ spectrum of the device in the 3D model under the tensile force in transverse direction with that in the two dimensional (2D) model. When there is a low transverse tension on the membrane $T_y = 0.03$ (dashed line), the peaks in the IL_∞ spectrum will shift to high frequency and the IL_∞ level drops below the criterion value of 9.6 dB. The lateral tension increases the membrane stiffness and restricts the motion of the membrane, which leads to undesirable performance. Such a trend of frequency shift and pattern can also be observed for 2D configuration of the theoretical model with $T_x = 0.07$ (dashed-dot line). The IL predicted in the 3D model for $T_x = 0.05$ and $T_y = 0$ (circle) matches well with that predicted in the 2D model for $T_x = 0.05$ (solid line). The modulus of the membrane modal coefficient $|V_{jl}|$ is shown in Figs. 5(c) and 5(d) as bar charts. Without tension $T_y = 0$, odd mode in the spanwise direction p are excited in the spanwise direction. The largest response in both cases is located near the second and fourth axial modes. When $T_y = 0$, Eq. (18) of the 3D problem can be reduced to two dimensions as

$$Z_{jj'} V_j = -(I_d + I_{d,\text{ref}})_j,$$

where $Z_{jj'} = \mathcal{L}_j + Z_{\text{rad},jj'} + Z_{\text{cav},jj'} + Z_{\text{ref},jj'}$.

The membrane vibration can be represented by the width-averaged velocity

$$V_w(x) = \frac{1}{w}\int_0^w V(x,y)\,dy = \sum_{j=1}^{\infty} V_j \sin(j\pi x/L),$$

and the complex amplitude of the radiated sound to the outlet

$$p_{\text{rad}}|_{m=0,x\to\infty} = \sum_{j=1}^{\infty} V_j R_j,$$

where R_j is the complex amplitude of the radiated wave by induced vibration of the jth mode with unit amplitude

$$R_j = \frac{1}{2}\int_{-L/2}^{L/2} \sin(j\pi\xi')e^{-ik_0 x_s} dx_s.$$

The conclusion is similar to that in Huang and Choy (2005). Therefore, based on the above analysis, the effect of the

lateral tension is eliminated in order to obtain the good performance and simplify the theoretical model.

E. Analysis of the IL peaks and troughs

In order to further investigate the sound radiation of the membrane, the modal response of the default membrane at the optimal performance ($m = 0.4$, $T_{opt} = 0.05$) is to be studied in this section. The IL spectrum is attached on the top of each column to facilitate the study of the peak and trough frequencies analyzed in Fig. 6. The vibration of each individual mode, $|V_j|$, is shown in the subfigures on the left column. The second column shows the amplitude of the modal radiation coefficient $|R_j|$, which characterizes the sound radiation ability from the membrane to the outlet of the duct. The third column is the amplitude of the single modal radiation $|V_j R_j|$.

The last column indicates the modal contribution to the total sound radiation γ_j which is defined as $\gamma_j = \mathrm{Re}[V_j R_j \hat{p}_{\mathrm{rad}}/|p_{\mathrm{rad}}|]$ at the two outlets of the duct, where $\hat{p}_{\mathrm{rad}}$ is the complex conjugate of p_{rad}. As mentioned in Sec. III D, the membrane response is dominated by the even modes rather than the odd modes in the amplitude of the vibration. Therefore, here, only first two even modes are discussed.

The specific frequency points at which IL_∞ is the lowest or highest are indicated by vertical dashed lines and are analyzed. There are two sharp peaks in the second mode $|V_2|$ at $f = 0.044$ and 0.146, respectively, in Fig. 6(1a) and one peak in the fourth mode $|V_4|$ at $f = 0.146$ in Fig. 6(1b). These correspond to the frequencies of trough points in the IL_∞ spectrum. From the subfigures in the last column, it can be observed that there is a positive peak at $f = 0.044$ in Fig. 6(4a) and it means that there is a strong sound radiation from the second mode to two outlets of the duct. On the other hand, regarding the second IL trough point at $f = 0.146$, a negative peak is seen in Fig. 6(4a) and a positive peak in Fig. 6(4b). The intermodal coupling and cancellation between the second and the fourth modes are expected to dominate the IL_∞ pattern. As shown in Figs. 6(1a) and 6(1b), the amplitude of $|V_4|$ is much larger than that of $|V_2|$ when the frequency is beyond 0.12, although there can be some cancellation, the strong magnitude of the fourth mode $|V_4|$ still dominates the sound radiation. To sum up, the trough points in IL_∞ are attributed to the strong radiation of the sound from the membrane to the outlet of the duct due to the excessively high response of the second and fourth modes of vibration.

In order to understand the mechanism for the peaks of IL_∞, the modal impedance is decomposed and analyzed under the optimal condition with $m = 0.4$ and $T_{opt} = 0.05$. In fact, the cross modal coupling is very weak at low frequencies, so only the modal impedance Z_{22} and Z_{44} of the second and fourth modes are discussed in Fig. 7. The two subfigures on the left hand side are for the second mode reactance including the structural contribution, $\mathrm{Im}(Z_{22} + L_2)$. The dotted lines are the structural dynamics contribution of inertia and stiffness terms. The open circles indicate the *in vacuo* membrane modes at frequencies $f = j/(2L_c)T/m = 0.118$ and 0.236 for $j = 2$ and 4, respectively. At $f = 0.118$, the structural impedance for the second mode becomes zero. At $f = 0.08$ (IL peak), the structural impedance is also small. Near this point, owing to vanishing structural impedance, it is good for the radiated sound waves from dipole with antiphase relationship to penetrate into the cavity. Such penetration can create destructive interference and maintain a high level of IL_∞ at the frequencies between the two peaks. In contrast, the two trough points of IL_∞ can be attributed to the total zero impedance of the second and fourth mode at $f = 0.044$ [Fig. 7(c)] and $f = 0.13$ [Fig. 7(d)], respectively. Beyond the second trough in the IL_∞ spectrum, the near-zero IL is displayed. The reason is mainly due to the divergence of the cavity mode as shown in Figs. 7(a) and 7(b). The cavity will become very stiff and it is difficult for sound to penetrate. The membrane becomes rigid and behaves as part of the straight duct, thereby no IL is obtained.

The structural impedance of the membrane determines the sound penetration. However, the performance of the

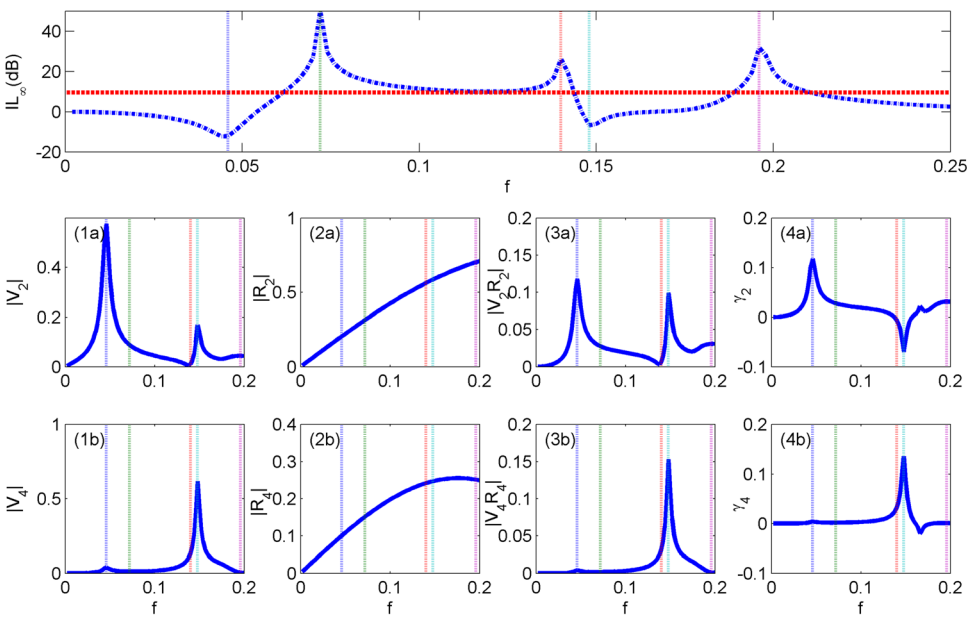

FIG. 6. (Color online) Modal radiations. The top figure is the IL spectrum at the optimal tension for the purpose of indicating the important dimensionless frequencies (f). The first column is the modal amplitude $|V_j|$, the second column is the modal radiation coefficient $|R_j|$, the third column is the single modal radiation $|V_j R_j|$, and the last column is the modal contribution γ_j.

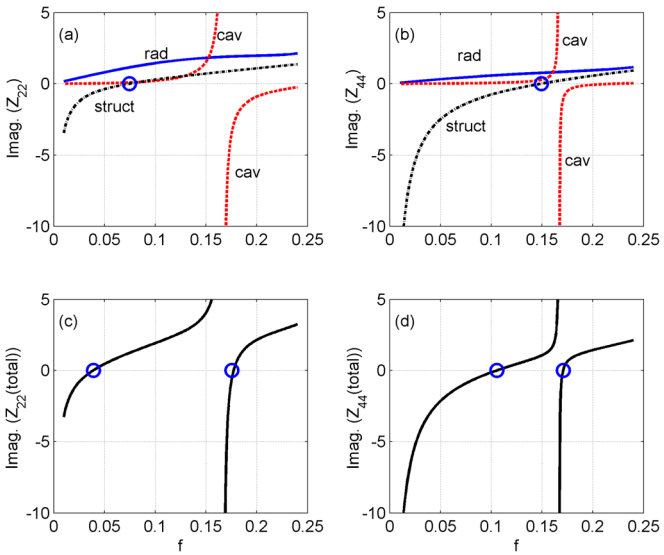

FIG. 7. (Color online) Reactance of the second and fourth modes. (a) shows the variation of the second mode component of imaginary part of impedance (Z_{22}) with dimensionless frequencies (f). Z_{rad} marked with "rad" (solid line), Z_{cav} marked with "cav" (dashed line), and $\mathcal{L}$ marked with "'struct" (dashed dotted line). (b) shows the fourth mode components of imaginary part of impedance (Z_{44}). (c) shows the total reactance of the second mode [Imag. (Z_{22})] and (d) shows the total reactance of the fourth mode [Imag. (Z_{44})] for which zero reactance is marked by an open circle.

device is also regulated by the sound coupling with the membrane response as well as its interference between the radiated sound from the membrane in the duct and the cavity, and the direct waves from dipole. Figure 8(b) compares the vibration velocity amplitude of the first two even modes, $|V_2|/|V_4|$, when $m = 0.4$ and $T_{opt} = 0.05$. The effect of the second mode decreases as the frequency increases. The second mode dominates the vibration for the frequency below $f = 0.114$, while the component of the fourth mode is prominent when f ranges from 0.114 to 0.184. The total sound pressure on the upper (p_{rad}) and lower surfaces (p_{cav}) of the membrane is expanded via a series of *in vacuo* modes with modal amplitude p_{radj} and p_{cavj} as $p = \sum_{j=1}^{N} p_j \sin(j\pi\xi)$, respectively. Then, the ratio of modal radiation pressure inside the main duct and cavity is expressed as $p_{radj}/p_{cavj} = |p_{radj}/p_{cavj}|e^{i(\theta_{radj}-\theta_{cavj})}$. The ratio of the magnitude of the pressure and phase difference between them for the second mode ($\theta_{rad2} - \theta_{cav2}$) and fourth mode ($\theta_{rad4} - \theta_{cav4}$) are plotted in Figs. 8(c) and 8(d), respectively. Below the first IL_∞ peak of $f = 0.07$, the phase difference for the second mode is zero. Near $f = 0.07$, there is a significant jump of ($\theta_{rad2} - \theta_{cav2}$) from zero to π. For the frequencies between the two peaks, the phase difference for the second and forth modes is kept at π, which means that the pressure on the upper and lower surfaces are out of phase, thus creating a destructive effect. Meanwhile, the ratio of the magnitude of the pressure $|p_{rad2}/p_{cav2}|$ and $|p_{rad4}/p_{cav4}|$ is also close to unity and this results in a good cancellation. At $f > 0.175$, only the fourth mode of vibration is dominant but the phase difference ($\theta_{rad4} - \theta_{cav4}$) drops to zero. This leads to a deterioration of the performance for higher frequency range.

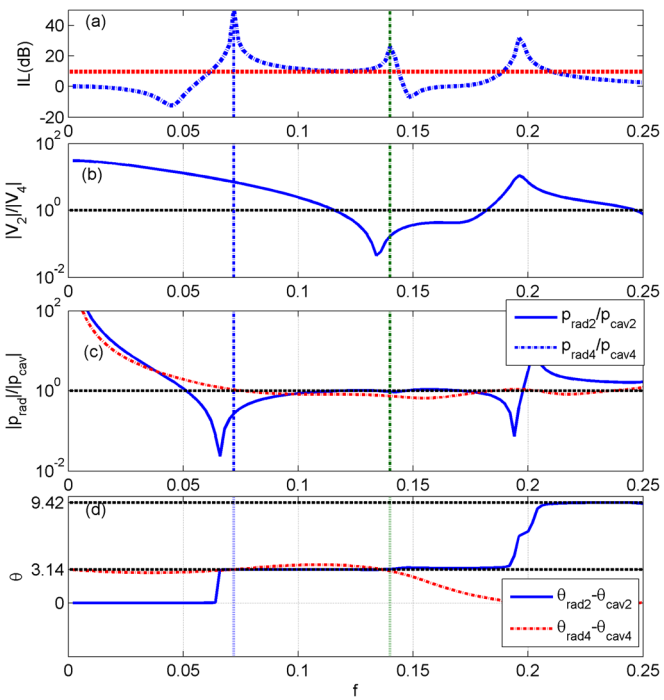

FIG. 8. (Color online) Relationship between second and fourth mode in vibration and pressure radiations at different dimensionless frequency (f). (a) IL spectrum of the optimal tension at the top is for clear illustration. (b) Vibration amplitude ratio of the second mode to the fourth mode. (c) Ratio and (d) phase difference of the pressure loading in the duct and cavity on the membrane.

F. Effect of the duct length

With open conditions at both ends of the duct, reflected waves are coupled with the vibrating membrane, thus compromising the performance of the silencer. Figure 9 shows the insertion loss spectra variations with different duct lengths with symmetrical upstream and downstream duct segments. With the fixed physical parameter of the membrane ($m = 0.05$ and $T = 0.4$), when the duct length at the upstream and downstream side of the membrane increases, the fluctuations of IL level appears to be more obvious. By comparing IL_∞ for the duct with infinite length without reflection sound waves, the IL patterns for the duct with

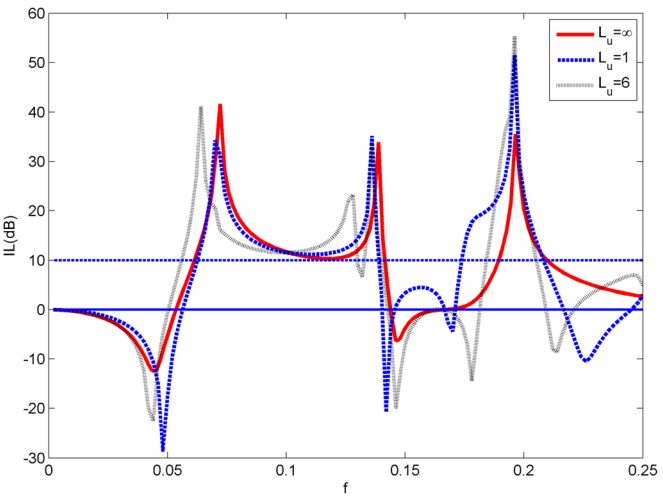

FIG. 9. (Color online) Variation of the IL against dimensionless frequency (f) for different duct lengths (dimensionless tension $T = 0.05$, mass ratio $m = 0.4$).

$L_u = 6$ and $L_d - L_c = 6$ with two peaks roughly around the frequencies of 0.07 and 0.136 are similar, but there is obvious deviation in the exact location of the peak and trough points as well as the stopband. The multiple reflections due to the two open end conditions form the standing waves that excite the membrane into vibration. This coupling between the dipole and standing waves as well as the vibration membrane obviously affects the sound cancellation between these sound waves. If the length of the duct at the downstream and upstream sides of the membrane is as short as $L_u = 1$, the trough points can be reduced so that the width of the stopband can be maintained desirably. Such spectral change for the variation of the length shows that this theoretical model taking into account the multiple reflections due to two open ends are necessary and useful to simulate the practical application with limited length or short length.

IV. CONCLUSIONS

Analyses have been conducted for the purpose of in-depth understanding of the sound-membrane coupling mechanism for the dipole source inside the tensioned membrane silencer in a 3D configuration. The performance of the cavity-backed tensioned membrane to control dipole sound source has been investigated by the analytical formulation. The optimization study has been conducted on several parameters such as the tension and the membrane mass. The fluid loading exerting on the membrane and the corresponding vibration response have also been analyzed in order to explain the IL_∞ pattern. Major conclusions can be drawn:

(i) With an appropriately determined low tension in the axial direction and zero tension in the lateral direction, the proposed device with tensioned membrane can achieve an IL_∞ higher than 10 dB over a frequency range with a stopband wider than an octave. Compared with that of an empty expansion chamber, the present device can achieve, on average, a 5 dB higher noise reduction in the frequency range of interest. Compared with a drum silencer, the optimal tension required is significantly lower and the length of membrane is shorter, which means that the present device will be more attractive to be used in applications.

(ii) The performance of such device relies on the destructive interference between the radiated waves from the membrane and direct waves from the dipole source via the vibroacoustic coupling. The response of the membrane plays a vital role to determine the whole sound and structural interaction process. With a dipole source, the second and fourth *in vacuo* modes of membrane dominate the vibration, as well as the suppression of the radiated noise from the dipole source.

(iii) The governing mechanism to control the dipole noise is to create the two antiphased waves undergoing destructive interference. The antiphased sound pressure at the top and bottom surface of the membrane undergoes sound cancellation. This is only possible when the structural impedance of the membrane is weak together with low radiation reactance. Therefore structural impedance plays a critical role in controlling the dipole sound radiation efficiency.

(iv) Experimental study has demonstrated that the proposed 3D theoretical model with limited duct length agrees well with the experimental data. The measured spectral peaks and troughs and the pattern of the measured IL also matches with the theory although some of the experimental data show more rounded peaks and troughs than theoretical predictions apparently due to the damping at the lateral membrane edges in the experiment.

ACKNOWLEDGMENTS

Y.L. thanks the Hong Kong Polytechnic University for the research studentship and further support from a seed fund (HKPolyU A-SA-43).

Ackermann, U., and Fuchs, H.V. (**1989**). "Technical note: Noise reduction in an exhaust stack of a papermill," Noise Control Eng. J. **33**, 52–60.

Choy, Y. S., and Huang, L. (**2002**). "Experimental studies of a drumlike silencer," J. Acoust. Soc. Am. **112**, 2026–2035.

Choy, Y. S., and Huang, L. (**2005**). "Effect of flow on the drumlike silencer," J. Acoust. Soc. Am. **112**, 3077–3085.

Doak, P. E. (**1973**). "Excitation, transmission and radiation of sound from source distributions in hard walled ducts of finite length. I. The effects of duct cross-section geometry and source distribution space time pattern," J. SoundVib. **31**, 1–72.

Dunne, R. C., and Howe, M. S. (**1997**). "Wall-bounded blade tip vortex interaction noise," J. Sound Vib. **202**, 605–618.

Ffowcs Williams, J. E., and Hall, L. H. (**1970**). "Aerodynamic sound generation by turbulent flow in the vicinity of a scattering half-plane," J. Fluid Mech. **40**, 657–670.

Fuchs, H. V. (**2001a**). "From advanced acoustic research to novel silencing procedures and innovative sound treatments," Acustica **87**, 407–413.

Fuchs, H. V. (**2001b**). "Alternative fiberless absorbers—New tools and materials for noise control and acoustic comfort," Acustica **87**, 414–422.

Huang, L. (**2002**). "Model analysis of a drumlike silencer," J. Acoust. Soc. Am. **112**, 2014–2025.

Huang, L., and Choy, Y. S. (**2005**). "Vibroacoustics of three-dimensional drum silencer," J. Acoust. Soc. Am. **118**, 2313–2320.

Huang, L., Ma, X., and Feng, L. G. (**2010**). "Suppression of broadband noise radiated by a low-speed fan in a duct," J. Acoust. Soc. Am. **128**, 152–163.

Kuttruff, H. (**2000**). "The sound field in a closed space (wave theory)," in *Room Acoustics* (E & FN Spon, New York), Chap. 3.

Lawrie, J. B., and Guled, I. M. M. (**2006**). "On tuning a reactive silencer by varying the position of an internal membrane," J. Acoust. Soc. Am. **120**, 780–790.

Levine, H., and Schwinger, J. (**1948**). "On the radiation sound from an unflanged circular pipe," Phys. Rev. **73**, 383–406.

Munjal, M. L. (**1987**). "Design of muffler," in *Acoustics of Ducts and Mufflers* (Wiley, New York), Chap. 8.

Rodarte, E., and Miller, N. R. (**2001**). "Modeling flow-induced noise of circular cylinders subject to cross flow inside a rectangular duct," in *Flow Induced Noise in Heat Exchangers ACRC-CR42* (University of Illinois, Champaign), Chap. 3.

Selamet, A., Xu, M. B., Lee, I.-J., and Huff, N. T. (**2005**). "Analytical approach for sound attenuation in perforated dissipative silencers with inlet/outlet extensions," J. Acoust. Soc. Am. **117**, 2078–2089.

Sharland, I. J. (**1964**). "Sources of noise in axial flow fans," J. Sound Vib. **1**, 302–322.

Wang, C. Q., Han, J., and Huang, L. (**2007**). "Optimization of a clamped plate silencer," J. Acoust. Soc. Am. **121**, 949–960.

Wang, J., and Huang, L. (**2006**). "Active control of drag noise from a small axial flow fan," J. Acoust. Soc. Am. **120**, 192–203.

Wang, J., Huang, L., and Cheng, L. (**2005**). "A study of active tonal noise control for a small axial flow fan," J. Acoust. Soc. Am. **117**, 734–743.

Zha, X., Fuchs, H. V., and Drotleff, H. (**2002**). "Improving the acoustic working conditions for musicians in small spaces," Appl. Acoust. **63**, 203–221.